Journal of Advanced Marine Engineering and Technology, Vol. 49, No. 6, pp. 525~535, 2025
J. Advanced Marine Engineering and Technology (JAMET)
https://doi.org/10.5916/jamet.2025.49.6.525

ISSN 2234-7925 (Print)
ISSN 2765-4796 (Online)
Original Paper

Integral sliding mode control for ship main cooling systems

Tae-youl Jeon[1] · Sun-tae Kim[2] · Young-chan Lee[†]

(Received October 20, 2025 ; Revised November 18, 2025 ; Accepted December 11, 2025)

Abstract: This paper presents the design and implementation of integral sliding mode control (ISMC) for the main cooling systems of ships. A ship cooling system is critical for maintaining optimal operational temperatures and ensuring the efficiency and reliability of ship machinery. However, conventional PI control often struggles to minimize energy consumption while maintaining stability under nonlinear disturbances, whereas standard sliding mode control suffers from chattering that can damage actuators. The proposed ISMC-based method addresses the challenges posed by system uncertainties and external disturbances, which are common in marine environments. Through mathematical modeling and simulation, ISMC is shown to save more energy than traditional control methods. These results indicate that seawater pumps are efficiently operated by ISMC. This study contributes to the advancement of control strategies in marine engineering and offers a viable solution for optimizing ship cooling systems.

Keywords: Sliding mode control, Energy efficiency, Ship main cooling system, Integral sliding mode control

1. Introduction

1.1 Research Background and Motivation

As energy efficiency and emissions reduction have emerged as critical challenges in the maritime and shipbuilding industries, the integration of the control and operation of auxiliary ship systems has become increasingly influential in shaping the overall energy profile and reliability of ships **[1][2][3][4]**. In particular, the proliferation of electric propulsion and shipboard microgrids has made the management of voltage quality and system stability necessary to mitigate rapid, short-term load fluctuations **[5][6]**. Consequently, it is essential to ensure sufficient safety margins through real-time control interventions.

As shown in **Figure 1**, the main cooling system plays a vital role in ensuring the thermal safety of engines and power electronic devices. This system is a multi-input single-output (MISO) system because of the combined effects of several interacting factors, including the operation of variable-speed seawater pumps and three-way valves, nonlinear heat transfer characteristics of the heat exchanger, temperature disturbances at seawater and freshwater inlets, and equivalent time delays from pipelines and sensors. Therefore, a control strategy that considers both temperature-tracking performance and energy consumption (seawater pump power) is required. However, traditional PI or internal model control (IMC) methods struggle to stably handle disturbances and uncertainties while meeting saturation constraints **[7]**.

Sliding mode control (SMC), a representative method in robust control, provides structural robustness against matched uncertainties and has been systematically extended to nonlinear systems through the fuzzy Takagi–Sugeno model **[8][9][10][11]**. Furthermore, theoretical and design frameworks that incorporate practical constraints such as output feedback, actuator saturation, state delays, and singular system dynamics have been developed, broadening the applicability of SMC to real-world processes, plants, and transportation systems **[12]**.

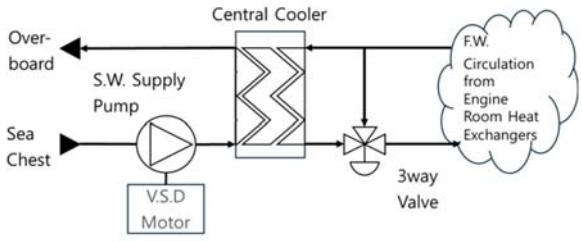

Figure 1: Main cooling system

† Corresponding Author (ORCID: http://orcid.org/0000-0002-3063-3285): Professor, Division of Coast Guard Studies, Korea Maritime & Ocean University, 727, Taejong-ro, Yeongdo-gu, Busan 49112, Korea, E-mail: yclee@kmou.ac.kr, Tel: 051-410-4661
1 Professor, Division of Marine System Engineering, Korea Maritime & Ocean University, E-mail: terry.jeon@kmou.ac.kr, Tel: 051-410-4573
2 Professor, Korea Institute of Maritime and Fisheries Technology, E-mail: lovejs@seaman.or.kr

This is an Open Access article distributed under the terms of the Creative Commons Attribution Non-Commercial License (http://creativecommons.org/licenses/by-nc/3.0), which permits unrestricted non-commercial use, distribution, and reproduction in any medium, provided the original work is properly cited.

Copyright ⓒ The Korean Society of Marine Engineering

Recent process control studies have introduced data-driven robust control schemes that also combine fuzzy neural network identification, sliding observers, and disturbance observers to dynamically estimate and compensate for disturbances while adaptively tuning the switching gains **[13][14]**. Such developments provide a solid foundation for addressing the variations in thermal–hydraulic nonlinear coupling and disturbances caused by changes in navigation conditions.

The main cooling system of a ship inherently involves nonlinearity and model mismatch, disturbances (e.g., seawater/freshwater temperature and engine load variations), time delays, and actuator saturation with output constraints. Therefore, the development of a control strategy that simultaneously achieves stable and energy-efficient operations is required.

1.2 Previous Studies and Limitations of Existing Controllers

Traditional PI and IMC-based cooling controllers frequently perform poorly when faced with model discrepancies or fluctuations in disturbances. These types of controllers often cause considerable overshoot during transient responses, steady-state errors, and energy waste due to unwarranted pump overflows. The presence of actuator saturation and time delays necessitates cautious tuning, which ultimately reduces performance **[15][16]**.

SMC provides strong tracking performance and robustness against matched uncertainties; however, its discontinuous switching action causes chattering, which may accelerate the wear of valves or pump components and introduce undesirable noise and vibration. To mitigate these issues, smooth control methods, higher-order sliding surfaces, and adaptive gain-adjustment techniques have been proposed. However, overestimation of the disturbance magnitude can still lead to unnecessary switching activities and energy waste **[17][18]**.

The integral SMC (ISMC) approach introduces an integral term into the sliding surface to eliminate steady-state error and ensure bounded state behavior under model uncertainties **[19][20]**. Nevertheless, several challenges remain when these methods are applied to real systems. Specifically, the controller must simultaneously address actuator saturation, variable time delays, and complex nonlinear thermal-hydraulic coupling.

To handle actuator saturation and output constraints, output-feedback SMC and singular value decomposition-based dimensionality reduction techniques have been proposed **[21][22]**. However, their experimental validation remains insufficient in complex environments such as marine cooling systems, where multiple interacting variables and nonlinear constraints coexist.

For systems with time delays and singularities, stabilization methods based on vector integral sliding surfaces have also been proposed **[23]**. Although theoretically effective, few studies have experimentally validated these methods in scenarios with multiple delay sources, such as thermal inertia, sensor delays, and pipeline transport delays while maintaining the system state on the sliding surface.

Additionally, methods that smoothly approximate actuator saturation and guarantee fixed-time convergence have been presented. However, research applying these approaches to thermo-fluid coupled systems, where thermal and flow dynamics are interdependent, or analyzing them from an energy consumption perspective, remains limited **[24]**. Furthermore, although adaptive SMC techniques that ensure the stability and continuity of the sliding manifold under time-delay conditions have been explored, further investigation is required to generalize them to distributed delay and multi-disturbance environments, such as marine cooling networks.

Consequently, an experimentally validated integrated control framework that simultaneously addresses the practical operational conditions and navigation disturbances of the main cooling system of a ship while achieving both temperature regulation and power reduction is lacking.

1.3 Research Objective

This research focused on creating a control framework that enhances the performance and energy efficiency through simulations utilizing real temperature disturbance data from an actual shipping route, shown in **Figure 2**.

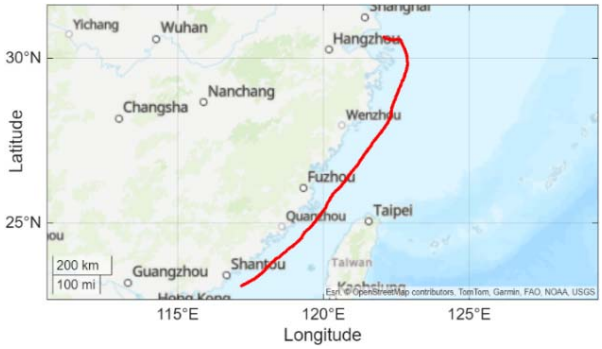

Figure 2: Ship navigation route

The proposed approach employs ISMC to eliminate steady-state errors and maintain stable operation within defined limits amid model uncertainties. It also ensures resilience against input discrepancies and matched uncertainties. By integrating an integral sliding surface with a departure-prevention control law that accounts for response delays and dynamic constraints, the proposed framework ensures both the reachability and stability of the closed-loop system.

2. Methodology

The mathematical representation of the system includes the nonlinear dynamics of the cooling mechanism to precisely depict its performance across different operating scenarios. The symbols, notation, and subscripts used in the mathematical model are listed in **Table 1**.

Table 1: Symbols, notations, and subscripts

Symbol	Description
Variables	
(t)	Lumped uncertainty (disturbances & model error)
e, e_1, e_2	Temperature tracking errors
$E(t)$	Total energy consumption
f_m	Power-supply frequency of seawater-pump motor (Control Input)
l_{3v}	Three-way valve stem position (Control Input)
$\dot{m}_s$	Seawater mass flow rate
$\dot{m}_f$	Freshwater flow rate supplied to the heat exchanger
$\dot{m}_{fin}$	Total freshwater mass flow rate
$\dot{m}_{by}$	Bypass mass flow rate through the 3-way valve
$P(t)$	Instantaneous electric power consumption
$s(t)$	Sliding surface function
T_f	Heat exchanger freshwater outlet temperature
T_f^*	Desired freshwater outlet temperature
T_{out}	Freshwater outlet temperature (after 3-way valve)
T_{out}^*	Desired outlet temperature of 3-way valve
T_{fin}	Freshwater inlet temperature
T_{sin}	Seawater inlet temperature
Parameters	
A	Heat-exchanger surface area
c_{pf}	Specific heat of freshwater
c_{ps}	Specific heat of seawater
ϵ, k	Sliding mode controller gains
E	System Gain constant
K_{3v}	Gain between valve-stem displacement and freshwater flow
K_{sp}	Gain between motor rotational speed and pump flow rate
$\lambda, \lambda_{1,2}$	Slope of sliding surface (tuning parameter)
ϕ	Saturation limit (boundary layer thickness)
$sign()$	Sign function
$sat()$	Saturation function
U	Overall heat-transfer rate of heat exchanger
Subscript	Meaning
$*$	Desired / Reference
$1, 2$	Indices for states or errors
$3v$	Three-way valve
by	Bypass
eq	Equivalent control input for Sliding Mode Control
in	Inlet
f	Freshwater
l	Lyapunov
m	Motor
out	Outlet
sp	Supply Pump
s	Seawater
sw	Switching control input for Sliding Mode Control

2.1 Seawater Pump and Three-Way Valve

In the initial model, it is assumed that the flow rate of the seawater supply pump is directly related to its rotational speed, while any time delays induced by piping and other components are ignored. The pump operates via an induction motor, and its rotational speed fluctuates based on the supply frequency from the electric power source. Assuming that the density of seawater remains constant, the correlation between the pump performance curve and motor frequency is derived in the following. First, the flow rate of the seawater supply is described by **Equation (1)**.

$$\dot{m}_s(t) = K_{sp} f_m(t) \tag{1}$$

Furthermore, as shown in **Figure 1**, the amount of freshwater flowing from the three-way valve to the heat exchanger is directly influenced by the valve opening, which varies with the stem movement of the three-way valve. When the total freshwater flow to the three-way valve remains constant, the flow rate to the heat exchanger can be represented by **Equation (2)**.

$$\dot{m}_f = K_{3v} l_{3v}(t) \tag{2}$$

Simultaneously, the rate of freshwater flowing past the heat exchanger is calculated by subtracting the amount supplied to the heat exchanger from the total freshwater flow entering the three-way

valve. This can be represented as **Equation (3)**.

$$\dot{m_{by}}(t) = \dot{m_{fin}} - K_{3v} l_{3v}(t) \tag{3}$$

Next, the outlet temperature of the central cooling system is established by combining the high-temperature freshwater flowing through the bypass side of the three-way valve with the cooled freshwater that has passed through the heat exchanger. The temperature variation within the three-way valve can be represented as the difference between the total thermal energy of the bypassed freshwater and heat-exchanged freshwater entering the valve and the thermal energy of the freshwater exiting the valve. This relationship can be described mathematically as **Equation (4)**.

$$m_{3v} c_{pf} \frac{dT_{out}(t)}{dt} = \dot{m_{by}} c_{pf} T_{fin}(t) + \dot{m}_f c_{pf} T_f(t) - \dot{m}_{fin} c_{pf} T_{out}(t) \tag{4}$$

The mathematical representation of the heat exchanger is subsequently formulated as two state equations. Based on the principle of energy conservation, the change in energy on the freshwater side corresponds to the difference between the energy that enters and exits the freshwater flow in addition to the energy conveyed to the seawater side via the heat exchanger.

Similarly, the change in energy on the seawater side is related to the disparity between the energy entering and leaving the seawater flow along with the energy moved from the freshwater side via the heat exchanger. These connections can be represented mathematically as shown in **Equations (5)** and **(6)**.

$$m_f c_{pf} \frac{dT_f(t)}{dt} = \dot{m}_f(t) c_{pf} \left(T_{fin}(t) - T_f(t)\right) - UA(T_f(t) - T_s(t)) \tag{5}$$

$$m_s c_{ps} \frac{dT_s(t)}{dt} = \dot{m}_s(t) c_{ps} \left(T_{sin}(t) - T_s(t)\right) - UA(T_f(t) - T_s(t)) \tag{6}$$

Assuming that the temperature distribution within the seawater is constant, with no changes in the internal seawater temperature, substituting **Equation (1)** into **Equation (6)** and rearranging the terms leads to **Equation (7)**.

$$T_s(t) = \frac{f_m(t) c_{ps} T_{sin}(t) + UAT_f(t)}{K_{sp} K_{sp} f_m(t) c_{ps} + UA} \tag{7}$$

By substituting **Equation (7)** into **Equation (5)** and organizing the terms concerning the variation in freshwater temperature, the resulting formula can be derived as **Equation (8)**.

$$\frac{dT_f(t)}{dt} = \frac{\dot{m_f}(t)}{m_f}\left(T_{fin}(t) - T_f(t)\right) - \frac{UAK_{sp} f_m(t) c_{ps}}{m_f c_{pf}\left(K_{sp} f_m(t) c_{ps} + UA\right)}\left(T_f(t) - T_{sin}(t)\right) \tag{8}$$

The rate of freshwater flow entering the heat exchanger, as defined in **Equation (2)**, can be integrated into **Equation (8)**, enabling it to be rearranged to create the first state equation, that is, **Equation (9)**.

$$\dot{T_f}(t) = \frac{K_{3v} l_{3v}(t)}{m_f}\left(T_{fin}(t) - T_f(t)\right) - \frac{UAK_{sp} f_m(t) c_{ps} m_f}{c_{pf}\left(K_{sp} f_m(t) c_{ps} + UA\right)}\left(T_f(t) - T_{sin}(t)\right) \tag{9}$$

By substituting **Equations (2)** and **(3)** into **Equation (4)** and organizing the terms according to the changes in the three-way valve outlet temperature, the resulting formula is the second state equation, which can be expressed as **Equation (10)**.

$$\dot{T_{out}}(t) = \frac{\dot{m_{fin}}}{m_{3v}}\left(T_{fin}(t) - T_{out}(t)\right) + \frac{K_{3v}\, l_{3v}(t)}{m_{3v}}\left(T_f(t) - T_{fin}(t)\right) \tag{10}$$

These two state equations describe the temperature dynamics of the freshwater and the mixed outlet, forming a nonlinear MISO thermal system.

To design the controller, the state-space form of **Equations (9)** and **(10)** can be expressed as

$$\dot{x} = f(x) + g_1(x) u_1 + g_2(x) u_2 + d(t) \tag{11}$$

where $x = \left[T_f, T_{out}\right]^T$, u_1 denotes the seawater pump frequency input, u_2 is the three-way valve opening, and $f(x)$ represents the uncontrolled system dynamics. In addition, $g_1(x)$ and $g_2(x)$ are functions that express the response of the system to control inputs u_1 and u_2, respectively. Finally, $d(t)$ represents temperature disturbances. This formulation enables the application of SMC theory described in the next section.

2.2 Definition of the Sliding Surface

An analysis of the state equations (**Equations (9)** and **(10)**) reveals that the system dynamics fluctuate based on the inputs and external

disturbances. Furthermore, this system is a MISO system, where the two control inputs consist of the power supply frequency for the seawater pump motor and the position of the three-way valve opening. Moreover, the single output is the freshwater outlet temperature from the three-way valve.

To simplify the control design, the control objectives are divided into two components, T_f^* and T_{out}^*, and a control strategy is designed such that T_f^* is equal to or lower than T_{out}^*. Since the target temperature is constant and the inlet freshwater and seawater temperatures, which act as disturbances, do not change abruptly, the sliding surface $s(t)$ is defined in terms of the temperature tracking error of the freshwater outlet temperature, as expressed in **Equation (12)**.

$$s(t) = e(t) + \lambda \int_0^t e(\tau)\, d\tau, e(t) = T_{\text{out}}(t) - T_{\text{out}}^* \tag{12}$$

Here, λ is a positive design parameter ($\lambda > 0$) that determines the bandwidth of the error dynamics on the sliding surface. When the system state reaches the sliding manifold (i.e., $s(t) = 0$), the error dynamics are governed by the first-order differential equation $\dot{e}(t) + \lambda e(t) = 0$. Consequently, λ dictates the exponential convergence rate of the temperature tracking error to zero. The reaching law adopts the exponential form in **Equation (13) [25]**,

$$\dot{s}(t) = -\epsilon\, sign\big(s(t)\big) - k\, s(t), \quad \epsilon > 0,\, k > 0, \tag{13}$$

which is standard in SMC.

2.3 Controller

2.3.1 Control Input for the Three-Way Valve

The control input is decomposed into an equivalent part and a switching part as follows:

$$u(t) = u_{eq}(t) + u_{sw}(t). \tag{14}$$

Differentiating the sliding surface based on **Equation (12)** gives

$$\dot{s}_1(t) = \dot{T}_{out}(t) + \lambda_1(T_{out}(t) - T_{out}^*) = 0. \tag{15}$$

By setting $T_{\text{out}}(t) = T_{\text{out}}^*$ in **Equation (10)** and substituting $\dot{T}_{\text{out}}(t)$into **Equation (15)**, we solve for the equivalent input (valve stem position) as **Equation (16)**.

$$l_{3v}^{eq}(t) = \frac{1}{K_{3v}\left(T_f(t) - T_{fin}(t)\right)} \dot{m}_{fin}\left(T_{out}(t) - T_{fin}(t)\right) - \frac{m_{3v}}{\lambda_1}\left(T_{out}(t) - T_{out}^*\right) \tag{16}$$

Using **Equation (10)** together with **Equation (13)**, the reaching (switching) component for the three-way valve becomes **Equation (17)**.

$$l_{3v}^{sw}(t) = -\frac{m_{3v}}{K_{3v}\left(T_f(t) - T_{fin}(t)\right)}(\varepsilon_1\, sign(s(t)) + k_1 s(t)) \tag{17}$$

To assess stability under parameter mismatch or unmodeled dynamics, let the lumped uncertainty be $\Delta(t)$. Then, the reaching dynamics are expressed as **Equation (18)**.

$$\dot{s}_1(t) = -\varepsilon_1\, sign(s_1(t)) - k_1 s_1(t) + \Delta(t) \tag{18}$$

Given the Lyapunov candidate $V_\ell(s_1) = \frac{1}{2}s_1^2$, its derivative is **Equation (19)**.

$$\dot{V}_\ell = s_1\dot{s}_1 = -k_1 s_1^2 - \varepsilon_1 \mid s_1 \mid + s_1\Delta(t) \tag{19}$$

Hence, if $\varepsilon_1 > \sup \mid \Delta(t) \mid$, then $\dot{V}_\ell < 0$for $s_1 \neq 0$, guaranteeing global asymptotic convergence to the sliding manifold.

2.3.2 Motor Supply Frequency Input for the Seawater Pump

The supply frequency channel adopts the same structure as that in **Equation (14)**, with the sliding surface defined as in **Equation (20)**.

$$\dot{s}_2 = \dot{e}_2 + \lambda_2 e_2 = \dot{T}_f + \lambda_2(T_f - T_f^*) = 0 \tag{20}$$

On the sliding manifold, the equivalent motor frequency is the value that makes $\dot{T}_f = 0$. Setting $\dot{T}_f = 0$ in Equation (9) and solving for $f_m(t)$ obtains **Equation (21)**.

$$f_m^{eq}(t) = \frac{1}{K_{sp}c_{ps}} \frac{UA(T_f^* - T_{sin}(t)) - K_{3v}l_{3v}(t)c_{pf}(T_{fin}(t) - T_f^*)}{UA + K_{sp}f_m(t)c_{ps}} \tag{21}$$

$$f_m^{eq}(t) = \frac{1}{K_{sp}c_{ps}} \frac{UA(T_f^* - T_{sin}(t)) - K_{3v}l_{3v}(t)c_{pf}(T_{fin}(t) - T_f^*)}{UA + K_{sp}f_m(t)c_{ps}} \tag{21}$$

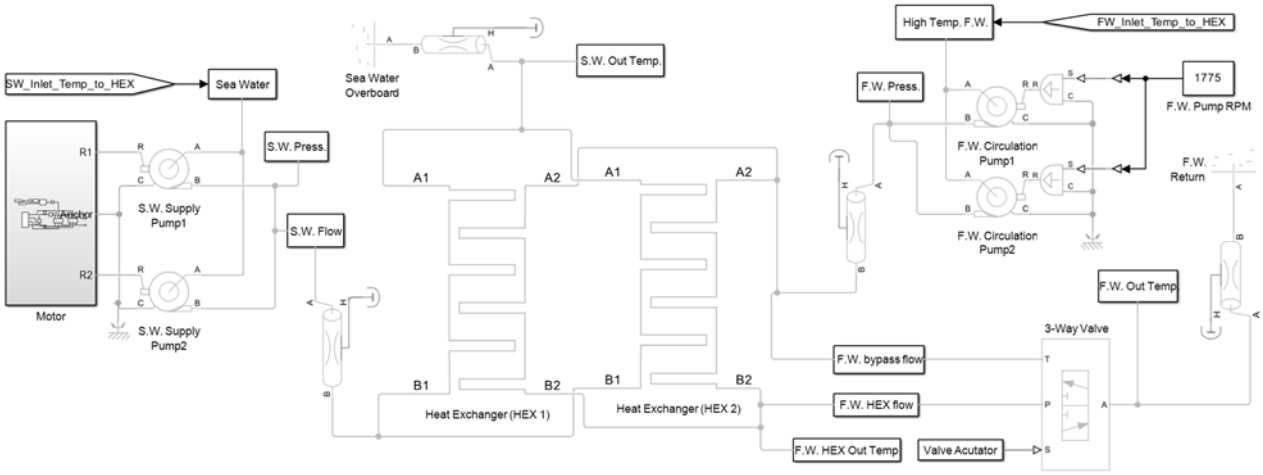

Figure 3: Simulink simulation model. S.W.: seawater; F.W.: freshwater

By substituting **Equation (9)** into the time derivative of sliding surface $\dot{s}_2$ and applying the partial derivative with respect to f_m in **Equation (21)**, we obtain the sensitivity function $G(f_m)$ as shown in **Equation (22)**.

$$G(f_m) = \frac{\partial \dot{s}_2}{\partial f_m} = \frac{\partial \dot{T}_f}{\partial f_m} = \frac{UA\,K_{sp}c_{ps}}{m_f c_{pf}\,(K_{sp}f_m c_{ps} + UA)^2}(T_{sin} - T_f) \tag{22}$$

Using the exponential reaching law

$$\dot{s}_2(t) = -\varepsilon_2\, sign(s_2(t)) - k_2 s_2(t), \varepsilon_2 > 0, k_2 > 0 \tag{23}$$

and a first-order approximation $\dot{s}_2 \approx G(f_m)\, f_m^{sw}$, the switching component for the motor frequency becomes **Equation (24)**.

$$f_m^{sw}(t) = -\frac{m_f c_{pf}\,(K_{sp}f_m(t)c_{ps} + UA)^2}{UA\,K_{sp}c_{ps}\,(T_{sin}(t) - T_f(t))}(\varepsilon_2\, sign(s_2(t)) + k_2 s_2(t)) \tag{24}$$

To prevent chattering in the switching input of the power frequency of the seawater supply pump, the discontinuous sign function in **Equation (24)** is replaced with a continuous saturation function, as expressed in **Equation (25)**, thereby smoothly approximating the switching region.

$$\mathrm{sgn}(s) = \begin{cases} -1, & s < -\Phi \\ \dfrac{s}{\Phi}, & |s| \le \Phi \\ +1, & s > \Phi \end{cases} \tag{25}$$

With Lyapunov function $V_\ell = \frac{1}{2}s_2^2$, we have

$$\dot{V}_\ell = -k_2 s_2^2 - \varepsilon_2 \mid s_2 \mid + s_2\, \Delta(t), \tag{26}$$

where $\Delta(t)$represents modeling errors or disturbances. Thus, if $\varepsilon_2 > \sup \mid \Delta(t) \mid$, then $\dot{V}_\ell < 0$, and the state reaches the sliding manifold and remains there. The final frequency command to the seawater-pump drive is the sum

$$f_m(t) = f_m^{eq}(t) + f_m^{sw}(t). \tag{27}$$

Consequently, f_m is determined based on the inlet freshwater temperature, inlet seawater temperature, and three-way valve opening.

3. Simulation

3.1 Model

The simulation model was implemented in MATLAB/Simulink, as shown in **Figure 3**, which replicates the main cooling system of an actual ship. The model configuration follows the practical layout described in **[26]**.

The setup includes two heat exchangers, a three-way valve, and a pair of seawater supply pumps. Each pump and heat exchanger can manage 50% of the designated load, allowing both units to function simultaneously. The speeds of both seawater-supply pumps is regulated using a single controller. Figure 4 shows the variable-speed motor drive incorporated in the model. While the actual ship utilizes induction motors for the seawater supply pumps, a DC power supply library block was implemented to facilitate electrical power calculations.

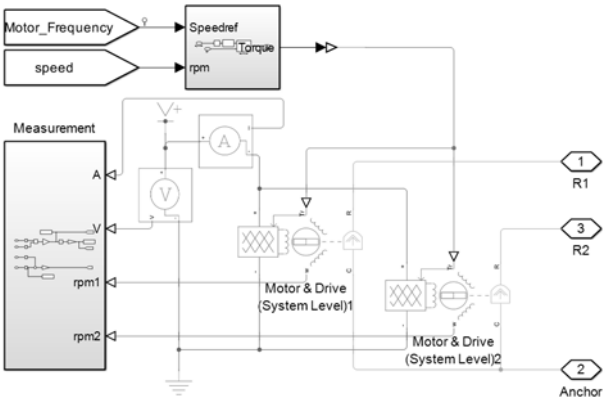

Figure 4: Seawater supply pump motor driver part

The connections between the motor speed, current usage, and torque were defined using the data sheet of the 45 kW, 4-pole, 60 Hz seawater-pump motor from the modeled vessel. Consequently, the parameters in the Motor & Drive (System Level) blocks shown in **Figure 4** were configured as reported in **Table 2**, and the minimum supply frequency was set to 30 Hz, in alignment with the reference vessel.

Because the supply voltage in the model is DC, the instantaneous electrical power and total consumed energy are calculated using **Equations (28)** and **(29)**, respectively.

$$P(t) = V(t)I(t) \tag{28}$$

Table 2: Parameter settings of the motor and drive model

Parameter	Value	Unit
Continuous operation maximum torque envelope	242.22, 242.22, 242.22, 242.22, 242.22, 120.00, 0	N · m
Corresponding rotational speed	0, 900, 1260, 1530, 1710, 1775, 1800	rpm
Torque control time constant	0.02	s
Motor and driver overall efficiency	93.6	%
Speed at which efficiency measured	1775	rpm
Torque at which efficiency measured	242.22	N · m
Iron losses	1	kW
Fixed losses	0.8	kW
Rotor inertia	0.546	kg · m^2
Rotor damping	0.02	N · m · s/rad

Table 3: Parameter settings of the heat exchanger model

Parameter	Value	Unit
Wall thermal resistance	2.53×10^{-7}	K/W
Wall mass	407	kg
Wall specific heat	523	J/K · kg
Minimum free-flow area	6.38×10^{-2}	m^2
Hydraulic diameter for pressure loss	6.92×10^{-3}	m
Thermal liquid volume	0.1355	m^3
Heat transfer surface area	90.4	m^2
Liquid-wall heat transfer coefficient	1.4×10^{4}	W/m^2 · K
Fouling factor	1.06×10^{-5}	m^2 · K/W

$$E(t) = \int_0^t P(\tau)\, d\tau \tag{29}$$

The heat exchanger was modeled based on the manufacturer's data sheets using the Heat Exchanger (Thermal Liquid–Thermal Liquid) block in Simulink. Its parameter settings are listed in **Table 3**.

3.2 Simulation Conditions and Controller Parameters

The simulation utilized the system model illustrated in **Figure 3**, which was executed in MATLAB/Simulink 2025a. The overall duration of the simulation was 48 h, representing the equivalent ship operation time. The primary goal of the cooling system control was to sustain a steady freshwater outlet temperature of 36 °C.

The freshwater and seawater inlet temperatures, acting as disturbances, were varied according to the real ship operational data, as shown in **Figure 5**. In this study, rather than changing the reference temperature, these two inlet temperatures were used as

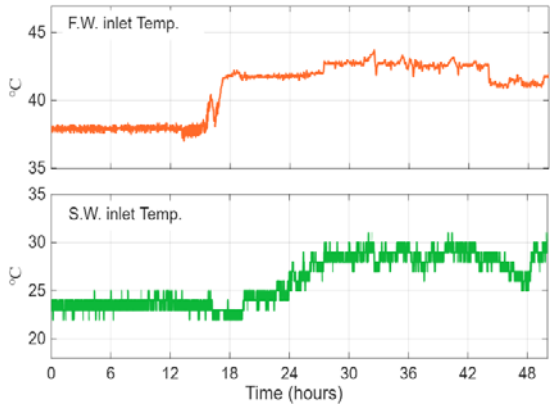

Figure 5: Operational data of freshwater (F.W.) and seawater (S.W.) inlet temperatures

Table 4: Parameters of PI-PI controller

Controller	K_P	K_I
S.W. supply pump	-548.8	-6.1
3-way valve	-13.1	-0.1

Table 5: Parameter values for SMC

Parameter	Value	Unit
U	16670	$W/m^2 \cdot K$
A	180.8	m^2
c_{pf}	4180	$J/kg \cdot K$
c_{ps}	3990	$J/kg \cdot K$
K_{sp}	3.8	$kg/s \cdot Hz$
K_{3v}	0.553	$kg/s \cdot mm$
m_{3v}	10	kg
$\dot{m}_{fin}$	110.66	kg/s
T^*_{out}	36	℃
T^*_f	36	℃

time-varying disturbance inputs to evaluate the robustness of the controller under realistic operating conditions.

Two controller types were applied and compared under identical environmental conditions. First, a PI–PI controller was designed using the IMC tuning method to ensure simple implementation and stable response characteristics. Second, an ISMC was developed based on the mathematical model derived in Section 2 with the aim of enhancing robustness against parameter uncertainties and external disturbances.

The performance comparison of these two controllers focused on three key aspects. First, the freshwater outlet temperature response was examined to evaluate control accuracy and stability. Second, the rotational speed and corresponding power consumption of the seawater-supply pump motor were analyzed to assess energy efficiency. Finally, the stem displacement of the three-way valve was monitored to evaluate the actuator effort and mechanical stability of the system.

The PI–PI controller was tuned according to the IMC method proposed by Jeon and Jung **[26]**. The gains listed in **Table 4** were selected to achieve a stable closed-loop response without excessive overshoot while ensuring sufficiently fast recovery from load disturbances.

The ISMC parameters are listed in **Table 5**. The values of the heat transfer coefficients, heat exchanger area, fluid properties, and mass flow rates were determined using the manufacturer's data sheets and the design specifications of the modeled vessel.

4. Simulation Result

Figure 6 shows the changes in the temperature of the freshwater outlet, along with the fluctuations related to the freshwater and seawater inlet temperatures. At the beginning of the simulation, the freshwater inlet temperature was roughly 38 °C, and after approximately 16 h, it surpassed 40 °C, ultimately reaching 43 °C. The seawater inlet temperature began at approximately 24 °C and steadily increased to approximately 30 °C after 18 h of operation. This movement aligns with the transition of the vessel from latitudes greater than 30° N to less than 25° N, as indicated by the navigation route shown in **Figure 2**.

The temperature of the freshwater outlet was maintained at 36 °C using both the traditional PI–PI controller and the ISMC. A slight rise followed by a drop in the outlet temperature can be observed around the 32-h and 40-h marks. This pattern occurs because, as illustrated in **Figure 7**, the seawater pump motor achieved its peak speed during these times, and **Figure 8** indicates that the three-way valve was fully extended (200 mm). As a result, the heat exchanger functioned at its maximum capacity and reached its thermal transfer threshold.

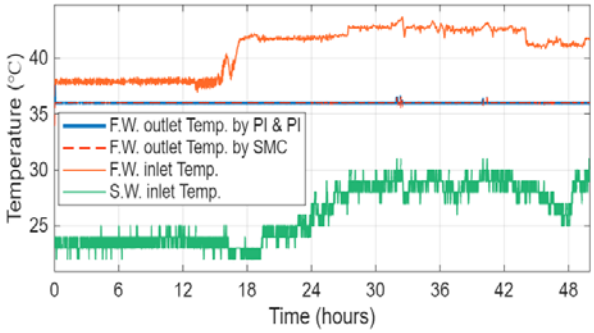

Figure 6: Controlled freshwater outlet temperature

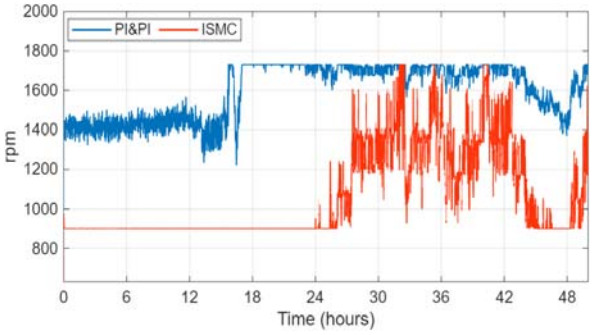

Figure 7: RPM of the seawater supply pump motor

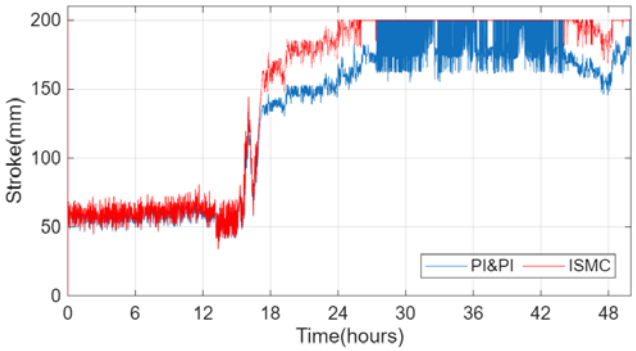

Figure 8: Stem stroke of the three-way valve

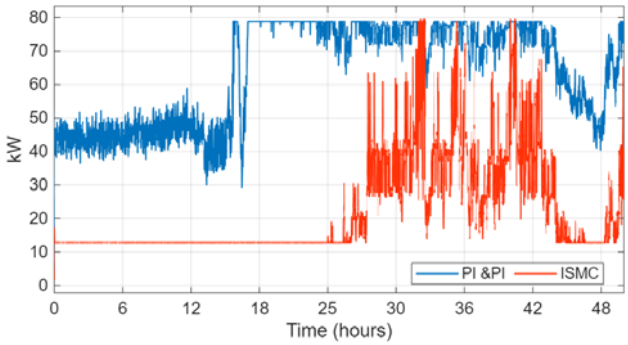

Figure 9: Electric power consumption of the seawater supply pump motor

Figure 9 illustrates the electrical power usage of the seawater-pump motor under both control strategies. When ISMC was used, the pump commenced operation at its lowest rotational speed, and as the thermal load on the heat exchanger increased from 16 h to 24 h, the opening of the three-way valve increased proportionately. After 24 h, the rotational speed of the seawater pump began to elevate, resulting in an increase in power consumption, as depicted in **Figure 9**.

In contrast, when the PI–PI controller was used, the seawater-pump motor ran at approximately 1400 rpm from 0 h to 14 h, using nearly 40 kW, and then functioned close to its peak speed, drawing approximately 80 kW. The overall electric energy usage of the seawater-pump motor was calculated using **Equation (31)** for the entire 48-h duration of the simulation.

The findings indicate that the overall energy usage with the proposed ISMC was 1103.2 kWh, and that of the PI–PI controller is 3194.9 kWh. Consequently, ISMC attained an energy-saving benefit of roughly 65% (equating to a decrease of 2091.7 kWh) relative to standard control, all while keeping the outlet temperature consistently at 36 °C. These findings indicate that ISMC has the ability to reliably manage temperature and increase energy efficiency by adjusting the pump speed and valve position in response to fluctuating thermal loads, even when faced with real-world ship navigation challenges.

5. Discussion and Conclusion

In this study, an ISMC model was implemented for the main cooling system of a ship to address the shortcomings of the traditional IMC-based PI-PI controller and to enhance both temperature stability and energy efficiency. The designed controller considers the nonlinear heat-transfer properties of the heat exchanger, the temperature fluctuations of seawater and freshwater, and the actuator saturation limits for both the pump and valve. To minimize chattering due to abrupt switching, a saturation function was utilized instead of a sign function, facilitating smoother control transitions. The simulation results indicate that the load on the seawater pump was reduced, and over a period of 48 h, the overall power consumption dropped from 3194.9 kWh (PI–PI control) to 1103.2 kWh, which is a 65% decrease. This illustrates that the proposed ISMC can concurrently achieve temperature-control stability and energy savings within a marine cooling system. The enhancements in performance are attributed to the incorporation of an integral term in the sliding surface, which removes steady-state deviations resulting from model discrepancies or disturbances, as well as the application of a saturation function that alleviates discontinuities in the control input. Moreover, by coordinating the pump frequency and the opening of the three-way valve, the system operates close to the optimal point for energy-efficient performance.

Nevertheless, this study has several limitations. The proposed controller was primarily validated through simulations based on MATLAB/Simulink; although actual operational data were used in the simulation, there was no real-ship validation. Additionally, because the parameters employed in the simulation were tailored to a specific ship's cooling system setup, their applicability to different vessel types and operational scenarios has not been evaluated. Furthermore, the applied disturbances were primarily based on route-specific temperature changes, thus necessitating further validation under various simultaneous disturbances and load variations. Future research will concentrate on overcoming these limitations via hardware-in-the-loop experiments and data-driven parameter-estimation methods, allowing adaptable compensation for system uncertainties. The proposed ISMC framework will also be broadened to an integrated optimal control design that merges the energy management systems of ship microgrids with propulsion and auxiliary systems. In summary, this study demonstrated the effectiveness of ISMC for a ship's main cooling system, which achieved both resilient temperature

tracking and substantial energy savings under realistic conditions. Although the validation is confined to a single ship model, the findings imply that the proposed method offers a promising basis for the advancement of digital twin-based marine energy management systems in future intelligent vessels.

Acknowledgement

This paper was supported by Korea Maritime & Ocean University (Development of Education and Training Platform for Disaster Response based on Virtual Convergence Technology) funded by Korea Government (Korea Coast Guard) in 2025 [No. 00254475].

Author Contributions

Conceptualization, T. Y. Jeon; Methodology, S.T. Kim and T. Y. Jeon; Software, T. Y. Jeon; Formal Analysis, T. Y. Jeon; Investigation, S.T. Kim; Resources, T. Y. Jeon; Data Curation T. Y. Jeon; Writing-Original Draft Preparation, S.T. Kim; Writing-Review & Editing, Y.C. Lee and S.T. Kim; Visualization, S.T. Kim; Supervision, author's name; Project Administration, Y.C. Lee; Funding Acquisition, Y.C. Lee.

References

[1] A. I. Ölçer, "Introduction to maritime energy management," Trends and Challenges in Maritime Energy Management, vol. 6, A. I. Ölçer, M. Kitada, D. Dalaklis, and F. Ballini, Eds., in WMU Studies in Maritime Affairs, vol. 6. , Cham: Springer International Publishing, 2018, pp. 1–12. doi: 10.1007/978-3-319-74576-3_1.

[2] C. A. Frangopoulos, "Developments, trends, and challenges in optimization of ship energy systems," Applied Sciences, vol. 10, no. 13, p. 4639, 2020.

[3] V. J. Jimenez, H. Kim, and Z. H. Munim, "A review of ship energy efficiency research and directions towards emission reduction in the maritime industry," Journal of Cleaner Production, vol. 366, p. 132888, 2022.

[4] Ó. A. Sanabria Vargas, H. D. Vergara Pestana, R. R. Mendoza Iglesias, and G. G. Salas Berrocal, "Electrical design for efficiency: technical and operational measures for optimizing the use of electrical power on ships," Ship Science & Technology, vol. 17, no. 33, pp. 33-41, July 2023.

[5] M. Cupelli, *et al.*, "Power flow control and network stability in an all-electric ship," Proceedings of the IEEE, vol. 103, no. 12, pp. 2355-2380, 2015.

[6] M. Farasat, A. S. Arabali, and A. M. Trzynadlowski, "A novel control principle for all-electric ship power systems," in 2013 IEEE Electric Ship Technologies Symposium (ESTS), Arlington, VA: IEEE, pp. 178-184, 2013.

[7] L. Seungtaek, L. Hoseang, and K. Hyeonju, "Dynamic simulation of system performance change by PID automatic control of ocean thermal energy conversion," Journal of Marine Science and Engineering, vol. 8, no. 1, p. 59, 2020.

[8] Q. Gao, L. Liu, G. Feng, Y. Wang, and J. Qiu, "Universal fuzzy integral sliding-mode controllers based on T–S fuzzy models," IEEE Transactions on Fuzzy System, vol. 22, no. 2, pp. 350–362, 2014.

[9] S.-C. Qu and Y.-J. Wang, "Fuzzy sliding mode control for uncertain nonlinear systems," Fuzzy Systems and Knowledge Discovery, vol. 3613, L. Wang and Y. Jin, Eds., in Lecture Notes in Computer Science, vol. 3613, Berlin, Heidelberg: Springer Berlin Heidelberg, 2005, pp. 960-968.

[10] Q. Gao, G. Feng, and Y. Wang, "A new robust sliding mode control scheme for uncertain T-S fuzzy systems," in 2013 IEEE International Conference on Fuzzy Systems (FUZZ-IEEE), Hyderabad, India: IEEE, pp. 1–6, 2013.

[11] J. Wang, Y. Wang, X. He, and S. Huang, "Fuzzy sliding mode tracking control for a class of uncertain nonlinear systems," Bio-Inspired Computational Intelligence and Applications, vol. 4688, K. Li, M. Fei, G. W. Irwin, and S. Ma, Eds., in Lecture Notes in Computer Science, vol. 4688, Berlin, Heidelberg: Springer Berlin Heidelberg, 2007.

[12] M. Tomar, M. S. Khan, R. K. Mandava, and D. G. Babu, "A review on sliding mode controller in real-time applications," 2022 IEEE International Students' Conference on Electrical, Electronics and Computer Science (SCEECS), BHOPAL, India: IEEE, pp. 1-6. 2022.

[13] X. Guo, C. Zhang, H. Zhang, S. Han, S. K. Kommuri, and Z. Wang, "Data-driven ensemble optimal compensation control for partially known delayed and persistently disturbed nonlinear systems," Journal of the Franklin Institute, vol. 361, no. 6, p. 106706, Apr. 2024.

[14] H.-G. Han, Y.-Q. Xing, and H.-Y. Sun, "Adaptive robust fuzzy sliding mode control for wastewater treatment processes," IEEE Transactions on Fuzzy Systems, vol. 32, no. 8, pp. 4787-4798, Aug. 2024.

[15] R. Ben Ali, E. Aridhi, and A. Mami, "Comparison between PID and predictive controllers applied to a cooling system," Water-Energy-Nexus in the Ecological Transition, V.

Naddeo, K.-H. Choo, and M. Ksibi, Eds., in Advances in Science, Technology & Innovation, Cham: Springer International Publishing, 2022, pp. 475-478, 2022.

[16] Y.-L. Chang and C.-C. Tsai, "Adaptive generalised predictive temperature control for air conditioning systems," IET Control Theory Applications, vol. 5, no. 6, pp. 813-822, Apr. 2011.

[17] S. Mahieddine-Mahmoud, M. Ouriagli, L. Chrifi-Alaoui, and P. Bussy, "Robust control of nonlinear systems with both matched and unmatched disturbances," 18th Mediterranean Conference on Control and Automation, MED'10, Marrakech, Morocco: IEEE, pp. 1043-1048, 2010.

[18] S. Das Mahapatra, R. Saha, D. Sanyal, A. Sengupta, U. Bhattacharyya, and S. Sanyal, "Designing low-chattering sliding mode controller for an electrohydraulic system," 2016 IEEE First International Conference on Control, Measurement and Instrumentation (CMI), Kolkata: IEEE, pp. 316-320, 2016.

[19] M. T. Hamayun, C. Edwards, and H. Alwi, "Integral sliding mode control," Fault Tolerant Control Schemes Using Integral Sliding Modes, vol. 61, in Studies in Systems, Decision and Control, vol. 61. Cham: Springer International Publishing, pp. 17-37, 2016.

[20] L. Peng, M. Jianjun, G. Lina, and Z. Zhiqiang, "Integral terminal sliding mode control for uncertain nonlinear systems," 2015 34th Chinese Control Conference (CCC), Hangzhou, China: IEEE, pp. 824-828, 2015.

[21] P. Xie and W. Liu, "An efficient approach to stabilization for linear systems subject to output saturation," Automatica, vol. 152, p. 110968, June 2023.

[22] K. Hui and C. W. Chan, "Multivariable saturation compensator designs through singular value decompositions," in Proceedings of the 1999 American Control Conference (Cat. No. 99CH36251), San Diego, CA, USA: IEEE, vol. 4, pp. 2506-2510, 1999.

[23] Y. Liu and S.-P. Ma, "A singular system approach to output feedback sliding mode control for time-delay systems: A singular system approach to output feedback sliding mode control for time-delay systems," Acta Automatica Sinica, vol. 39, no. 5, pp. 594-601, Mar. 2013 (in Chinese).

[24] S. S. Butt, R. Prabel, and H. Aschemann, "Robust input-output linearization with input constraints for an engine cooling system," 2014 American Control Conference, Portland, OR, USA: IEEE, pp. 4555-4560, 2014.

[25] J. Liu and X. Wang, Advanced Sliding Mode Control for Mechanical Systems. Berlin, Heidelberg: Springer Berlin Heidelberg, 2011.

[26] T.-Y. Jeon and B.-G. Jung, "A study of PI controller tuning methods using the internal model control guide for a ship central cooling system as a multi-input, single-output system," Journal of Marine Science and Engineering, vol. 11, no. 10, p. 2025, Oct. 2023.